An Experimental Study of the Antineutron-Light Nucleus Annihilation at 1.4 GeV/c

H.-J. Besch, H.W. Eisermann, G. Nöldeke, and W. Vollrath
Physikalisches Institut der Universität Bonn, Bonn

D. Waldren
CERN, Geneva

H. Kowalski
Deutsches Elektronen-Synchrotron DESY, Hamburg

H.-J. von Eyß and H. von der Schmitt*
Institut für Kernphysik der Universität Mainz, Mainz

The heavy liquid bubble chamber, Gargamelle, has been used to investigate the gross features of the annihilation of antineutrons in light nuclei (mainly Carbon). Results are presented on the distributions of multiplicity, momentum and emission angle for charged pions and protons together with a simple model to describe them.

In this paper we describe the results of an experiment performed to determine the gross features of the $\bar{n}$-light nucleus annihilation process. The distributions of i) multiplicity, ii) emission angle and iii) momentum have been determined for both charged pions and protons together with some correlations. The experiment was performed in the large heavy liquid bubble chamber Gargamelle.

The chamber, a cylinder of radius 1 m and length 4 m, situated in a magnetic field of 1.97 T, was filled with a propane-freon mixture of density 0.597 g cm^{-3}. The contributions of free protons, light nuclei (C, F) and heavy nuclei (Br) acting as targets for annihilation in this mixture are given in Table 1. A beam of antiprotons at momentum 1.6 GeV/c entered almost along the axis of the chamber, and approximately 250,000 pictures, containing on average three antiprotons were taken.

This paper is organized as follows. In Sect. 1 we describe the properties of the incident antineutron "beam". In Sect. 2 we give a general description of

Table 1. Composition of the chamber liquid (from Ref. 13) and contributions from the different nuclei to all annihilations. The cross sections are valid for antineutrons of 750 MeV kinetic energy [2, 12]. For Fluorine and Bromine they were calculated by the method described in Appendix A

Nucleus	% by weight	% by number	$\sigma_{ann.}$/mb	% annihil.
^{1}H	10.9	66.8	52	18
^{12}C	52.1	26.6	425	58
^{19}F	15.4	5.0	550	14
^{80}Br	21.6	1.6	1,230	10

our event sample. In Sect. 3 we present the results. In Sect. 4 we develop a simple intranuclear cascade type model for the description of the data and in Sect. 5 we give conclusions.

1. Properties of the $\bar{n}$ "Beam"

The antineutrons which were used for our investigation were produced in the charge exchange reaction

$$\bar{p}p \to \bar{n}n$$

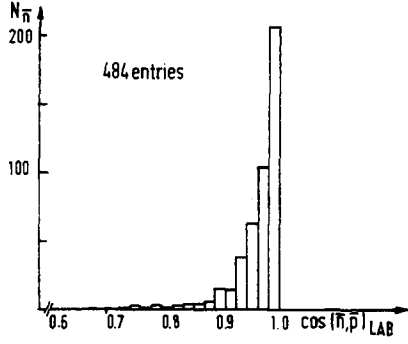* This work is based in part on the thesis by H. von der Schmitt (D 77)

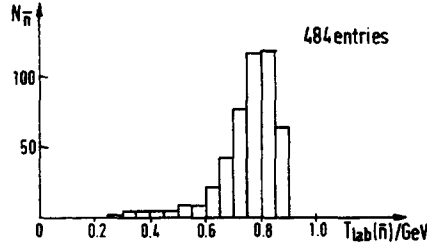**Fig. 1.** Angular distribution of antineutrons

Fig. 2. Kinetic energy distribution of antineutrons

which was observed together with the subsequent annihilation

$$\bar{n}A \rightarrow \text{all types of events.}$$

The data presented here are based on the full measurement of 484 events of this type. To exclude $\bar{n}$ coming from other reactions we demanded at the scanning stage to see the charge exchange vertex together with the downstream antineutron star. The annihilation star was further required to be separated from the charge exchange vertex by at least 5 mm on the projection table (corresponding to ~ 2 cm in space). The background due to the reactions

$$p\bar{p} \rightarrow n\bar{n} + m\pi^0, \qquad m \geqq 1$$

was excluded by the requirement of no γ rays pointing to the charge exchange vertex. This removes $\sim 85\%$ [1] of the single π^0 events and as the cross section for charge exchange with the production of one neutral pion is already small, the residual background due to this reaction is negligible. The probability of seeing at least one γ-ray for the reaction involving $2\pi^0$'s is 98% which excludes possible background due to the charge exchange reaction with many neutral pions.

The distribution of our measured $\bar{n}$ production angles is shown in Fig. 1. It peaks in a narrow forward cone as expected for charge exchange reactions. From two particle kinematics the energy of the $\bar{n}$ is computed for

each event and plotted in Fig. 2. The mean kinetic energy is 750 MeV. From the two possible solutions for the $\bar{n}$ momentum we chose the larger one since the smaller solution was always approximately 10 MeV/c. Such a slow $\bar{n}$ does not travel far enough before annihilating to pass the vertex separation cut made at the scanning stage.

2. Event Sample

We measured 484 events with 2,365 charged secondary tracks. Among these events we found 411 events with a total of 2,008 tracks with unambiguous mass and charge assignment (minimum ionizing positive tracks were considered for dynamical reasons as unambiguous π^+). These unambiguous 411 events were used for the determination of multiplicities, momentum and angular distributions. To correct this sample for possible event loss or contaminations we computed for each of these 411 events the relative weight according to the misidentification probability due to the following effects:

a) Tracks with secondary interactions near the annihilation vertex leading to a π^+/π^- ambiguity or even to a $\pi^+/\pi^-/p$ ambiguity; the corrections for this effect were determined with the help of the remaining 73 events of our sample where such secondary interactions were observed.

b) Misidentification of short stopping π^- as protons: this effect leads for example to the erroneous identification of the reaction $\bar{n}p \rightarrow \pi^+\pi^+\pi^-$ with π^- momentum below ~ 60 MeV/c as $\bar{n}A \rightarrow p\pi^+\pi^+$.

The distribution of the weights is shown in Fig. 3. The 411 weighted events were then used for the determination of multiplicities, momentum and angular distributions shown in Figs. 4-9.

It should be noted that we made no attempt to correct for the π/K misidentification, considering all non identified kaons as being pions. In our sample we expect around 50 kaons [2] from which we found only 5.

Events with the total charge $+1$ in which only pions were seen were classified as type $\bar{n}p$. It was impossible to distinguish whether an event of this type was an annihilation on a free proton or inside a nucleus. It can be estimated [3, 2] that most of $\bar{n}p$ type events were annihilations on free protons. Leaving out all of them would introduce a bias to the $\bar{n}A$ sample. We have attempted to correct for this measuring some number of $\bar{n}p$ type events. This number was chosen to be equal to the number of $\bar{n}n$ type events. The assumption was made that both types of annihilations occur with equal frequencies in the nucleus, and that the probability to produce no proton tracks
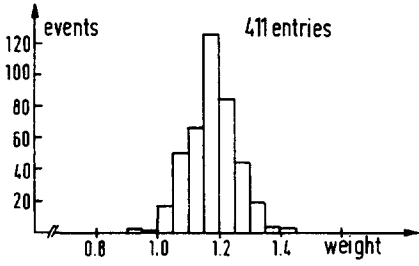
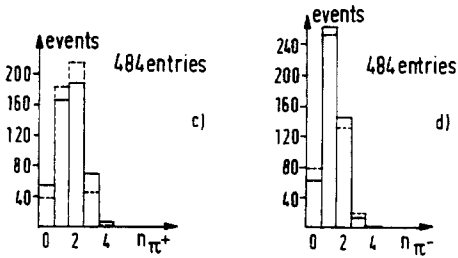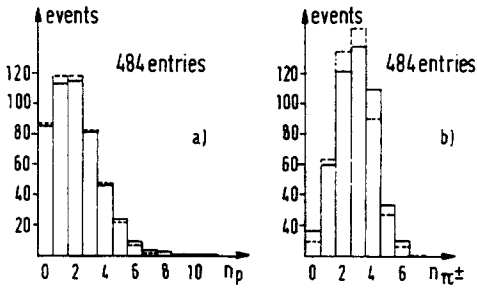Fig. 3. Distribution of the weights correcting experimental gain or loss of events of different topology

Fig. 4a–d. Multiplicity distributions of a protons, b pions and separately c π^+, d π^-. Dashed lines: results from model
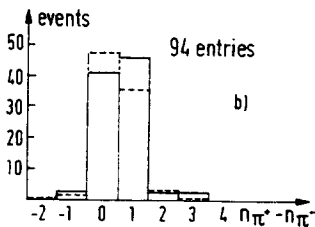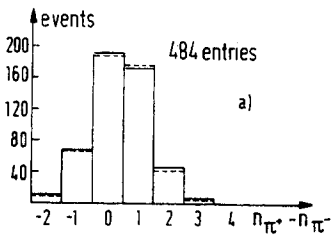

Fig. 5a and b. Distributions of the total pion charge $n_{\pi^+} - n_{\pi^-}$, a for all events, b for events without protons only. Dashed lines: results from model
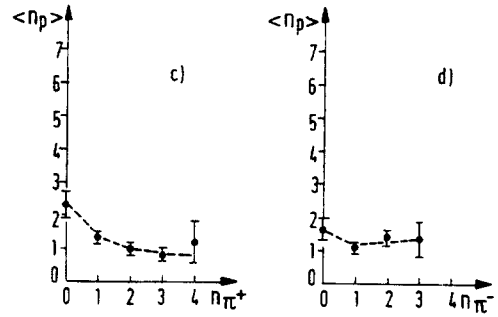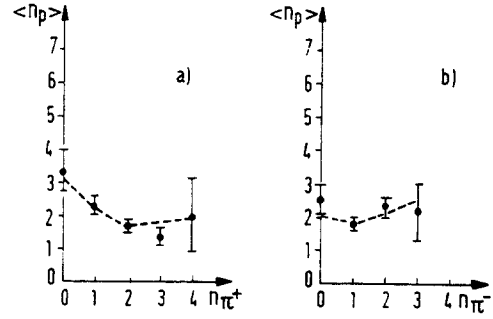

Fig. 6a–d. Correlations between pion and proton multiplicities. $\langle n_p \rangle$ vs. a n_{π^+} and b n_{π^-} for all protons, c and d accordingly for protons with momentum > 300 MeV/c only. Dashed lines: results from model

Fig. 7a and b. Kinetic energy distributions a for pions and b protons. The events of the $\bar{n}p$ type, which are mainly on Hydrogen, were excluded from the pion plot. Solid lines: results from model; dashed line in pion spectrum: distribution for annihilations on free nucleons

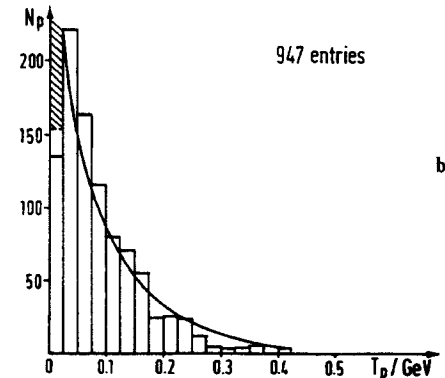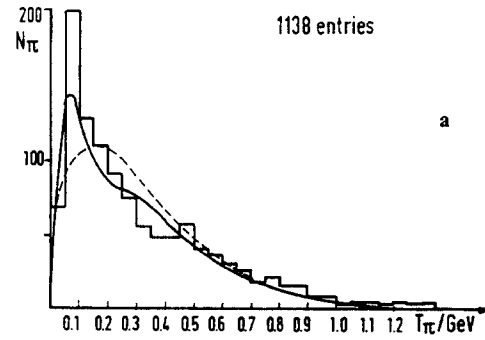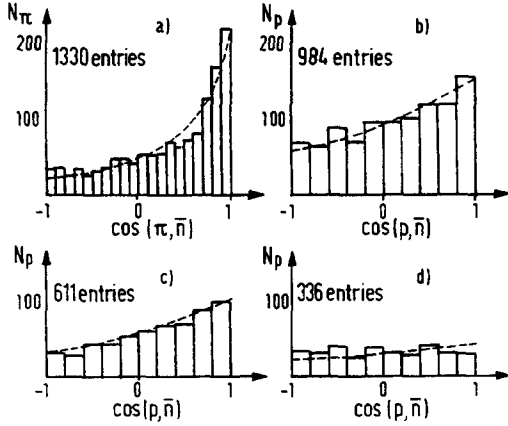Fig. 8a–d. Angular distributions of a pions and b protons, and separately for fast protons (momentum >300 MeV/c) (c) and slow protons (d). Dashed lines: results from model. The pion angular distribution in the annihilation on free protons is essentially identical to our model prediction
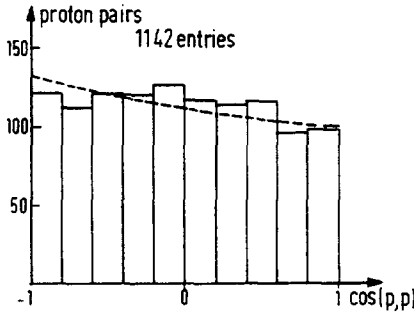

Fig. 9. Angular correlation between protons. Dashed line: results from model

is equal in both cases. Having adjusted the number of $\bar{n}p$ type events in this way, the fraction of events without protons becomes 0.19 ± 0.03.

3. Results

The measured multiplicity distributions are shown in Fig. 4 and compared to the multiplicities from annihilations on free nucleons in Table 2. The mean prong number is increased by ~ 1.5, resulting from a mean proton multiplicity of ~ 2.1 and a reduction of the mean charged pion number by ~ 0.6.

In Fig. 5 is plotted the total charge of the pions. For the events without proton tracks, practically only the charges 0 or 1 are observed, corresponding to annihilations of the $\bar{n}n$ or $\bar{n}p$ types. Correlations between pion and proton multiplicities are investigated in Fig. 6. The plots of the mean proton multiplicity vs. the π^+ multiplicity shows a negative correlation while there is no significant dependence between $\langle n_p \rangle$ and the π^- multiplicity.

Table 2. Mean multiplicities and energies

	$\bar{p}p$ [2] at rest	$\bar{p}p$ [1] 1.6 GeV/c	This expt. $\bar{n}A$ 1.4 GeV/c
$\langle n_{\pi^+ - o} \rangle$	5.02	5.43	–
$\langle n_{\pi^+ -} \rangle$	3.06	3.43	2.82 ± 0.07
$\langle n_{\pi^-} \rangle$	1.53	1.72	1.23 ± 0.04
$\langle n_p \rangle$	–	–	2.12 ± 0.09
$\langle T_\pi \rangle$	234 MeV	377 MeV	322 ± 8 MeV
$\langle T_p \rangle$	–	–	88 ± 2 MeV

The energy distributions of pions and protons are shown in Fig. 7. The mean kinetic energy of the pions is 322 ± 8 MeV. The protons have a mean energy of 88 ± 2 MeV. Protons with less than ~ 17 MeV are lost because their range in the liquid is shorter than 5 mm. Above 175 MeV (momentum: 600 MeV/c) some protons may be missing due to misidentification as π^+, because we have defined all weakly ionizing positive ambiguous tracks (163 tracks) to be pions. In Figs. 8a, b, c, d the pion and proton angular distributions are plotted.

We note that the distribution of energy and emission angle for pions resemble the corresponding distributions in the annihilation on free protons or neutrons, see Fig. 7a and 8a.

4. Description of Data in Terms of a Phenomenological Model

To describe the data on $\bar{n}$ annihilation in a nucleus we developed a simple Monte Carlo type model similar to intranuclear cascade models [4], which accounts for the main properties of observed distributions. (When we speak about annihilation in the nucleus we mean the annihilation in the various nuclei of the chamber filling, see also Appendix A.) Our model is based on the assumption that the $\bar{n}$-nucleus interaction is a two step process. In the first step, the $\bar{n}$ annihilates on one of the bound nucleons inside the nucleus which is assumed to have a smooth density distribution known from experiment [5] (see also Appendix A). In the second step the annihilation products reinteract inside the nucleus. We assume that the annihilation on bound nucleons is the same as annihilation on free ones. In the annihilation on free nucleons only pions are produced. Around 1.6 GeV/c incident momentum the average pion multiplicities are [1, 6]

$$\langle n_{\pi^+ -o} \rangle = 5.4 \quad \text{and} \quad \langle n_{\pi^+ -} \rangle = 3.4.$$

The angular and momentum distributions of annihilation pions are determined by phase-space in each

final multiplicity. In Table 2 we summarized the main results on annihilation of antiprotons on free protons relevant to our investigation. For antineutron-neutron annihilation we assumed that the process is the same as the antiproton-proton annihilation.

For the outgoing pions two reinteraction types were considered: a) absorption and b) scattering. Absorption is responsible for the reduction of the observed mean charge multiplicity in the annihilation from 3.43 ± 0.04 on free nucleons to 2.82 ± 0.09 on nuclei as observed in our experiment. This reduction cannot be due to the charge exchange reaction. The charge exchange reaction effects only slightly the charged pion multiplicity since the probability for π^0 to exchange charge inside the nucleus is approximately two times bigger than for charged pions and the ratio of charge to neutral pions in the annihilation is ~ 1.8 [1].

The effects of scattering show up mainly in the pion kinetic energy (or momentum) distribution. The primary distribution of pion kinetic energies annihilation on bound nucleons is compared with data in Fig. 7a.

From this figure it can be seen that the observed pions have, on the average, lower kinetic energy than the pions from the primary annihilation (dashed line). This effect can be understood as due to the elastic scattering of pions.

The absorption and scattering cross sections for pions in our energy region are strongly energy dependent due to the effects of the Δ-resonance. The Δ-resonance width in nuclear reactions is observed to be approximately 50% broader than in the scattering on free nucleons or absorption on free deuterons [7]. To take into account this broadening effect, which has not yet been well understood, we take as energy dependence for the elementary pion processes of absorption and scattering the shape of the pion reaction cross section observed on Carbon [7]. This cross section shows the Δ-resonance peak which is roughly 50% broader than the resonance in πN scattering.

After the pion production in the primary annihilation was simulated in the computer the path of each pion through the nucleus was followed. The pion reinteraction point was chosen according to the probability distribution

$$\exp\left(-\sigma(E_\pi)\int\rho(\lambda')\,d\lambda'\right)$$

where λ' parametrizes the path along the pion direction, $\sigma(E_\pi)$ denotes the absorption or scattering cross section and ρ is the nuclear density.
The cross sections for scattering and absorption were taken in the form

$$\sigma_s = a\sigma_\pi^{\text{reac}}, \qquad \sigma_{ab} = b\sigma_\pi^{\text{reac}}.$$

Here, a and b denote constants which were fitted to the data in such a way that the average charged pion multiplicity and the average pion kinetic energy were reproduced. The angular distribution for elastic scattering was parametrized in a similar way to that described in Ref. 4. In this way we obtained the mean pion scattering length in nuclear matter

$$\lambda_\pi^s \approx 2.1 \text{ fm}.$$

This value agrees well with the mean pion scattering length estimated from the elastic scattering on free nucleons. The predicted shape of the pion kinetic energy distribution with the elastic scattering switched on also agrees well with the observed one (see Fig. 7a).

The mean pion absorption length in nuclear matter was found to be

$$\lambda_\pi^{ab} = 7.5 \text{ fm}$$

and is also in reasonable agreement with the values obtained in other experiments [8]. In particular we computed, with our fitted absorption cross section, the $\pi^+ C$ total absorption cross section at $T_\pi = 130$ MeV and obtained $\sigma_{ab}^{\text{model}} = 156 \pm 5$ mb. This value should be compared with $\sigma_{ab}^{\text{exp}} = 189 \pm 19$ mb as observed in the experiment of Bellotti et al. [9]. The energy of the Bellotti et al. experiment lies in the region of strong energy dependence of the absorption cross section; nevertheless, we obtained a good agreement.

In our model protons are produced through scattering and absorption of pions. A scattered proton with energy greater than the binding energy was assumed to leave the nucleus. The mean number of protons knocked out by intranuclear scattering was found in the model to be $\langle n_p^s \rangle = 0.9$. The mean number of protons per event from absorption was then found to be $\langle n_p^{ab} \rangle = 1.25$ just giving together with $\langle n_p^s \rangle$ the observed mean proton number $\langle n_p \rangle = 2.12 \pm 0.09$. The mean number of protons per absorbed pion which was also found to be 1.3, is in good agreement with the measurement of Ballandin et al. [14], where $\langle n_p^{ab} \rangle \sim 1.6$ per absorbed pion (averaged over charge) was observed. We assumed further that absorbed pions give their energy to the whole nucleus which then emits nucleons in a statistical way with $\langle n_p^{ab} \rangle = \langle n_n^{ab} \rangle = 1.3$. The angular and momentum distributions were then obtained from phase-space. The distributions for all protons are compared to experiment in Figs 7b and 8b and agree very well. The small discrepancy between the predicted value for the mean proton kinetic energy (107 MeV) and the experimental one (88 ± 2 MeV) can be understood as a consequence of our decision to treat all tracks with moments above 600 MeV/c as pions.

Table 3. Comparison of the data about $\bar{p}$ annihilation at rest in different materials [10] with the predictions of our model

A	$\langle n_{\pi^-} \rangle$		$\langle n_{\pi^+} \rangle$		$\langle n_{\pi^{+-}} \rangle$	
	exp.	mod.	exp.	mod.	exp.	mod.
C	1.57	1.62	1.22	1.25	2.79	2.87
Ti	1.49	1.51	1.09	1.16	2.58	2.68
Ta	1.46	1.45	1.01	1.05	2.47	2.50
Pb	1.49	1.45	0.95	1.04	2.44	2.49

Table 4. Comparison of the data from the $\bar{p}$ annihilation in emulsion [11] with the predictions of our model

$\bar{p}$ incident momentum	$\langle n_{\pi^{+-}} \rangle$		$\langle T_\pi \pm \rangle$	
	exp.	model	exp.	model
At rest	2.61 ± 0.08	2.60	226 ± 8	222 MeV
In flight $\langle T_{\bar{p}} \rangle = 154$ MeV	2.34 ± 0.08	2.30	217 ± 11	229 MeV

Table 5. Predictions of the model for annihilation products multiplicities and energies in different nuclei at 1.4 GeV/c incident $\bar{n}$ momentum

	$\langle n_{\pi^{+-}} \rangle$	$\langle n_{\pi^+} \rangle$	$\langle n_{\pi^-} \rangle$	$\langle n_p \rangle$	$\langle T_\pi \rangle$	$\langle T_p \rangle$	N.S. prob.
C	2.80	1.60	1.20	2.03	321	105	80%
F	2.63	1.50	1.13	2.41	320	108	84%
Br	2.26	1.29	0.97	2.81	297	107	86%

N.S. (nuclear signature) probability denotes the percentage of events with at least one proton seen

Because of the large cross section of the annihilation process the antineutrons annihilate preferentially on the surface of the nucleus. This effect leads in turn to a deviation from isotropy in the angular distribution of protons (Fig. 8b), due to the fact that more pions are absorbed and scattered in the forward direction.

In our model we do not expect any angular correlation between protons since they are emitted in a statistical way. This is in agreement with the data (Fig. 9) and does not contradict the fact that normally such correlations are observed as a consequence of the quasideuteron pion absorption mechanism. As was observed by Bellotti et al. [9], only 10–20% of pions are absorbed through the quasideuteron mechanism. Such an amount of quasideuteron absorption would not lead to visible angular correlations between protons in our experiment.

The observed pion-proton multiplicity correlations, see Fig. 6, are due in our model to the conservation of energy and charge. Energy conservation tends to produce a negative correlation while charge conservation in the case of π^+ leads to negative and in

case of π^- leads to positive correlations. For π^-, both effects cancel.

In Tables 3 and 4 we show the comparison of the prediction of our model for mean charged pion multiplicity and energy with the data of other experiments on $\bar{p}$ annihilation in different nuclei and at different energies. The dependence of pion absorption from the target atomic number A can be tested with data of Bugg et al. [10], who measured the mean charged pion multiplicity for $\bar{p}$ annihilation at rest in C, Ti, Ta and Pb. The multiplicity is observed to decrease with increasing A. This effect has an obvious origin and is quantitatively well described by our model (see Table 3). The variation of the incident antiproton energy leads to two opposite effects: a) with increasing $\bar{p}$ energy the mean pion path length inside the nucleus increases, since the annihilation takes place on the average deeper in the nucleus, b) with the increasing $\bar{p}$ energy the annihilation pion energy grows and leaves the region of Δ-resonance reducing the absorption cross section quickly. The energy dependence can be tested with an emulsion experiment of Ekspong et al. [11], see Table 4 and is quantitatively well described by the model. Calculated results for the $\bar{n}$ annihilation on F and Br are given in Table 5.

5. Conclusion

In our experiment we investigated the gross features of annihilation of antineutrons in nuclei (mainly in Carbon). We determined the distribution of multiplicity, momentum and emission angle for charged pions and protons together with some correlations. The physical interest in this reaction lies in the fact that $\bar{n}$ annihilation acts as a pion factory inside the nucleus and sheds some light on the interaction of pions with nuclei. The data can be well described with the help of a simple, intranuclear cascade type model. We compared also the predictions of our model with the data of other experiments on $\bar{p}$ annihilation in different nuclei and at different energies. The agreement was also satisfactory.

Besides the interest in physics of antinucleon annihilation in nuclei our results can be useful for acceptance calculations for counter experiments detecting antineutrons by their characteristic annihilation. Such experiments are presently being performed at DESY and SLAC.

Appendix A

Determination of Total Annihilation Cross-Section on Different Nuclei

In our experiment the heavy liquid bubble chamber Gargamelle was filled with a propane-freon mixture.
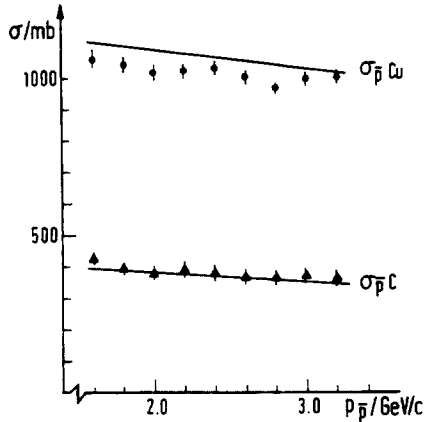
Fig. 10. Calculated $\bar{p}C$ and $\bar{p}Cu$ annihilation cross-sections (with error bars!) and measured values (full line!)

The percentages of Hydrogen, Carbon, Fluorine and Bromine in this mixture are given in Table 1. The total annihilation cross section in the energy region of our experiment has been measured in Hydrogen [2], Carbon and Copper [12]. To determine the relative probabilities for annihilation on Fluorine and Bromine we made the following simple computation.

We assumed that the nuclear matter density of nuclei $\rho(r)$ is given by

$$\rho(r) = \frac{0.169 \text{ nucleons/fm}^3}{1 + \exp((r - (c + \Delta c))/(0.35 \text{ fm}))}$$

where c denotes the half density radius determined in electron scattering [5], Δc denotes a constant which we add to the nuclear radii of C, F and Br, to take into account the strong interactions. Using the annihilation cross sections on free protons and neutrons we then computed the annihilation cross section on Carbon and fixed the value of Δc by fit to the data at 1.6 GeV/c incident $\bar{p}$ momentum. In this way we obtained $\Delta c = 0.6$ fm. The radius of Carbon obtained in electron scattering is 2.2 fm. With the constant Δc fixed, we computed the nuclear annihilation cross sections for Carbon and Copper at all energies at which the annihilation cross sections were measured by Abrams et al. [12]. The comparison to the data shows a good agreement, see Fig. 10. In the same way we computed the annihilation cross section for Fluorine and Bromine and determined then the percentages of annihilation on each of the target nuclei present in the Gargamelle filling. The results are given in Table 1.

References

1. Fett, E., Haatuft, A., Olsen, J.M., Hart, W., Knight, W.L., Madrolle, P., Waldren, D., Alibran, P., Degrange, B., Arnold, R., Engel, J.P., Guyonnet, J.L., Kurtz, N., de Unamuno, S.: Physics Lett. **59** B, 182 (1975)
2. Enstrom, J.E., Ferbel, T., Slattery, P.F., Werner, B.L., Guiragossián, Z.G.T., Sumi, Y., Yoshida, T.: $\bar{N}N$ and $\bar{N}D$ Interactions – A Compilation, LBL-58, Berkeley 1972
3. Montanet, L., in: von Dardel, G. (ed.): Proceedings of the Lund International Conference on Elementary Particles Held at Lund, Sweden, June 25–July 1, 1969, pp. 193–222. Lund: Berlingska Boktryckeriet 1969
4. Metropolis, N., Bivins, R., Storm, M., Turkevich, A., Miller, J.M., Friedlander, G.: Phys. Rev. **110**, 185 (1958)
   Chen, K., Fraenkel, Z., Friedlander, G., Grover, J.R., Miller, J.M., Shimamoto, Y.: Phys. Rev. **166**, 949 (1968)
5. Überall, H.: Electron Scattering from Complex Nuclei, Part A. New York and London: Academic Press 1971
6. The annihilation of $\bar{n}$ on protons leads around 1.6 GeV/c incident momentum to approximately the same charge and total pion multiplicity as in the $\bar{p}$ case, private communication of the group of Ref. 1
7. Hüfner, J.: Physics Reports **21** C, 1 (1975)
8. Gugelot, P.C., Kullander, S., Landau, G., Lemeilleur, F., Yonnet, J.: Nucl. Phys. B **37**, 93 (1972)
9. Bellotti, E., Cavalli, D., Mattenzzi, C.: Nuovo Cim. **18** A, 75 (1973)
10. Bugg, W.M., Condo, G.T., Hart, E.L., Cohn, H.O., McCulloch, R.D.: Phys. Rev. Lett. **31**, 475 (1973)
11. Ekspong, A.G., Frisk, Å., Nilsson, S., Ronne, B.E.: Nucl. Phys. **22**, 353 (1961)
12. Abrams, R.J., Cool, R.L., Giacomelli, G., Kycia, T.F., Leontic, B.A., Li, K.K., Lundby, A., Michael, D.N., Teiger, J.: Phys. Rev. D **4**, 3235 (1971)
13. GARGAMELLE User's Handbook, CERN Geneva
14. Balandin, M.P., Ivanov, O.I., Moiseenko, V.A., Sokolov, G.L.: Soviet Phys. JETP (USA) **19**, 279 (1964)

H.-J. Besch
H.W. Eisermann
G. Nöldeke
W. Vollrath
Physikalisches Institut
Universität Bonn
Nussallee 12
D-5300 Bonn
Federal Republic of Germany

D. Waldren
CERN
CH-1211 Geneva 23
Switzerland

H. Kowalski
Deutsches Elektronen-Synchrotron DESY
Notkestieg 1
D-2000 Hamburg 52
Federal Republic of Germany

H.-J. von Eyß
H. von der Schmitt
Institut für Kernphysik
Universität Mainz
Becherweg 31
D-6500 Mainz
Federal Republic of Germany